RSC Advances




ROYAL SOCIETY OF CHEMISTRY

www.rsc.org/advances

# Diorganotin(IV) 2-pyridyl and 2-pyrimidyl thiolates: Synthesis, structures and their utility as molecular precursors for the preparation of tin sulfide nanosheets

Adish Tyagi,[a] G. Kedarnath,*[a] Amey Wadawale,[a] Vimal K. Jain,*[a] Mukesh Kumar[b] and B. Vishwanadh[c]

[a]*Chemistry Division, Bhabha Atomic Research Centre, Mumbai- 400 085 (India),*
*Email: kedar@barc.gov.in; jainvk@barc.gov.in*

[b]*Solid State Physics Division, Bhabha Atomic Research Centre, Mumbai- 400 085 (India),*

[c]*Materials Science Division, Bhabha Atomic Research Centre, Mumbai- 400 085 (India).*

## Table of contents

Organotin complexes, $[R_2Sn(2\text{-}SC_5H_4N)_2]$ and $[R_2SnCl\{SC_4H(Me\text{-}4,6)_2N_2\}]$ (R = Me, Et) were prepared, characterized and utilized as ssps for the preparation of SnS nanosheets. The direct/indirect band gaps of the latter were evaluated.

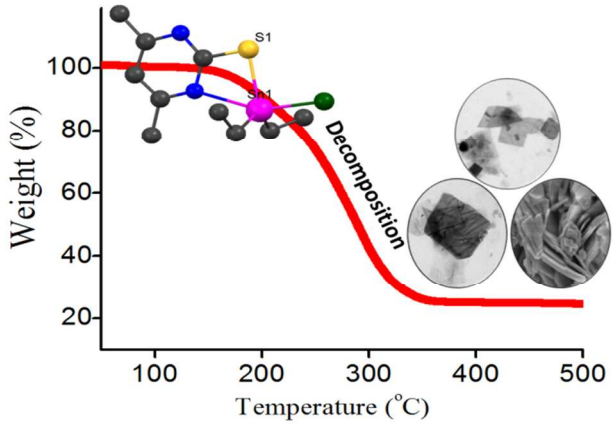


## Abstract

The complexes of composition, $[R_2Sn(2\text{-}SC_5H_4N)_2]$ (R = Me (**1**) or Et (**2**)), $[Et_2SnCl(2\text{-}SC_5H_4N)]$ (**3**) and $[R_2SnCl\{SC_4H(Me\text{-}4,6)_2N_2\}]$ (R = Me (**4**), Et (**5**)) were prepared and characterized by elemental analyses and NMR ($^1H$, $^{13}C$, $^{119}Sn$) spectroscopy. The molecular structures of $[Et_2Sn(2\text{-}SC_5H_4N)_2]$ (**2**), $[Me_2SnCl\{SC_4H(Me\text{-}4,6)_2N_2\}]$ (**4**) and $[Et_2SnCl\{SC_4H(Me\text{-}4,6)_2N_2\}]$ (**5**) were established unambiguously by single crystal X- ray diffraction analyses. The central tin atom acquires a skew trapezoidal bipyramidal configuration in the former (**2**) while distorted trigonal bipyramidal geometry in the latter two complexes (**4** and **5**), respectively. Thermolysis of diethyltin complexes $Et_2Sn(2\text{-}SC_5H_4N)_2]$

(**2**) and [$Et_2SnCl\{SC_4H(Me\text{-}4,6)_2N_2\}$] (**5**) in oleylamine (OLA) afforded orthorhombic phase SnS nano-sheets of thickness 30-80 nm which were characterized by solid state diffuse reflectance spectroscopy, XRD, EDX, SEM and TEM techniques. The solid state diffuse reflectance measurements of the nanosheets showed direct and indirect band gaps in the ranges of 1.61–1.90 eV and 1.46 eV, respectively which are blue shifted relative to bulk tin sulfide [$E_g$ (direct) = 1.3 eV and $E_g$ (indirect) = 1.1 eV)].

**Keywords:** Diorganotin complexes, 2-pyridylthiolate, 2-pyrimidylthiolate, NMR, tin sulfide, nanostructures, band gap

## Introduction

Research on binary compound semiconducting materials, IV-VI in their bulk and low dimensional forms have drawn significant attention due to their promising applications in optoelectronics[1,2] and thermoelectrics[3]. Among them, PbE (E = S or Se) are widely studied.[4-11] However, the toxic nature of lead restricts their environment friendly utilization of these materials. As an alternative, the focus is shifted to the materials such as tin sulfide containing benign, cheap, earth-abundant elements and having comparable optical properties to that of toxic counter parts.

Tin sulfide exists in three prominent forms [SnS ($E_g$ = 1.3 eV); $SnS_2$ ($E_g$ = 2.18 eV) and $Sn_2S_3$ ($E_g$ = 0.95 eV)][12] and exhibits excellent semiconducting properties. Tin sulfides have several applications in solar energy absorber,[13,14] infrared detecting,[15] holographic recording devices[16,17]. However, SnS due to its remarkable electronic properties received considerable attention. For example, SnS has a direct band gap (1.3 eV) which falls in the range between the band gaps of Si and GaAs, high absorption coefficient ($\sim 10^5$ $cm^{-1}$)[18] and hole concentration of $10^{18}$ $cm^{-3}$ and the Hall mobility (resistivity ~0.06 Ωcm) of 90 $cm^2$/Vs at room temperature[18].

To date several synthetic strategies have been reported for the preparation of tin sulfide nanostructures and thin films either in solution[19-25] or gas phase[26 -32]. The solution phase synthetic routes have distinct advantages of low production cost, easy processibility, phase purity, size and shape controllability while gas phase methods have better control over the reactions due to convenient supply and mixing of reactants, rate of reaction. Reaction can easily be controlled by temperature of substrate and reacting gases/vapor[33]. Although there are various solution and gas phase methods available for the preparation of tin sulfide nanostructures, single source precursor (ssp) route has an advantage over other methods due to its versatility. These precursors can be used to synthesize nanostructures adopting solution or wet chemical route and can also be utilized for the deposition of nano-structured thin films using aerosol assisted chemical vapor deposition (AACVD) method. In addition, the ssp route proved to be a better method to obtain phase pure and narrowly distributed nanostructures and also handling of

precursors is convenient compared to multiple source precursors. A number of ssps were used for deposition of tin sulfide thin films. Recently O'Brien *et*. al. deposited SnS thin films using tin thiosemicarbazone complexes of the type $Bz_3SnCl(L)$ (L = thiosemicarbazones of salicylaldehye and 4-chlorobenzaldehyde)[29] and diorganotin dithiocarbamates, $[Bu_2Sn\{S_2CN(RR')\}_2]$ (R, R′ = Et; R = Me, R′ = Bu; R, R′ = Bu; R = Me, R′ = hexyl) and $[Ph_2Sn\{S_2CN(RR')\}_2]$ (R, R′ = Et; R = Me, R′ = Bu; R, R′ = Bu; R = Me, R′ = hexyl)[34]. There are only two reports dealing with the utility of ssps for the preparation of nanostructures in solution.[35,36] Recently, we have employed 2-pyridyl- (**I**) and 2-pyrimidylchalcogenolate (**II**) of group 12, 13, 14 and 15 metals for the preparation of metal chalcogenide nanomaterials and for the deposition of thin films.[24-26]

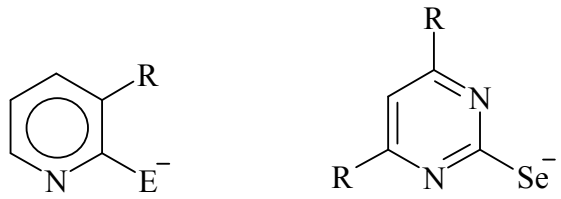


**I** **II**

(E = Se or Te; R = H or Me)

In view of the above and to develop ssp for the preparation of tin sulfide nanostructures, we have investigated the chemistry of organotin 2-pyridyl- and 2-pyrimidyl thiolate complexes. Accordingly, we have synthesized diorganotin(IV) complexes of 2-pyridyl- and 2-pyrimidylthiolate and utilized them as molecular precursors for the preparation of tin sulfide nanostructures (hexagonal and rectangular sheets, *etc*.). The results of this work are described herein.

## Experimental

### Materials and Methods

Diorganotin dichlorides ($R_2SnCl_2$; R = Me or Et,), oleylamine (OLA) and analytical grade solvents were obtained from commercial sources. The ligand, $[HSC_4H(Me\text{-}4,6)_2N_2]$ ($^1$H NMR ($D_2O$) $\delta$: 2.49 (s, Me); 6.94 (s, CH-5). $^{13}C\{^1H\}$ NMR ($D_2O$) $\delta$: 19.6 (Me); 111.5 (CH-5); 168.0 (C-2); 173.3 (C-4,6)) was prepared according to literature method.[37]

Elemental analyses were carried out on a Thermo Fischer Flash EA1112 CHNS analyzer. The $^1$H, $^{13}C\{^1H\}$ and $^{119}Sn\{^1H\}$ NMR spectra were recorded on a Bruker Avance-II NMR spectrometer operating at 300, 75.47 and 111.92 MHz, respectively. Chemical shifts are relative to internal chloroform peak for $^1$H and $^{13}C\{^1H\}$ NMR spectra, and 30% $Me_4Sn$ in $C_6D_6$ for $^{119}Sn\{^1H\}$ NMR spectra. Thermo gravimetric analyses (TGA) were carried out on a Nitzsch STA 409 PC-Luxx TG-DTA instrument, which was

calibrated with $CaC_2O_4.H_2O$. The TG curves were recorded at a heating rate of 10 $^oC$ $min^{-1}$ under a flow of argon. X-ray powder diffraction patterns were obtained on a Philips PW-1820 diffractometer using $CuK_\alpha$ radiation. Optical diffuse reflectance measurements in the 200−1800 nm (0.68 eV to 6.2 eV) regions were conducted on a two-beam spectrometer (V-670, JASCO) with a diffuse reflectance (DR) attachment consisting of an integration sphere coated with barium sulfate. $BaSO_4$ was used as a reference for the same. Measured reflectance data were converted to absorption (A) using Kubelka-Munk remission function[38]. The band gaps of the samples were estimated by extrapolating the linear portion of the plot to X (energy) axis. SEM and EDX measurements were carried out on ULTRA 55 FESEM of Zeiss and Oxford Inca instruments, respectively. Tecnai G2 T20 transmission electron microscopes operating at accelerating voltages up to 200 kV were used for TEM studies. The samples for TEM and SAED were prepared by placing a drop of sample dispersed in acetone/toluene on a carbon coated copper grid.

Intensity data for $[Et_2Sn(2\text{-}SC_5H_4N)_2]$ (**2**) were collected on a Agilent Super Nova microfucus X-ray source ($CuK_\alpha$, $\lambda$ = 1.5418 Å) radiation, $[Me_2SnCl\{SC_4H(Me\text{-}4,6)_2N_2\}]$ (**4**) and $[Et_2SnCl\{SC_4H(Me\text{-}4,6)_2N_2\}]$ (**5**) were collected on a Rigaku AFC7S diffractometer using graphite monochromated $MoK_\alpha$ ($\lambda$ = 0.71069 Å) radiation at room temperature (298 ± 2K) so that $\theta_{max}$ = 27.5$^o$. The unit cell parameters (Table 1) were determined from 25 reflections measured by a random search routine. The intensity data were corrected for Lorentz, polarization and absorption effects with an empirical procedure[39]. The structures were solved by direct methods using SHELX-97[40] and refined by full-matrix least squares methods. The non-hydrogen atoms were refined anisotropically. The hydrogen atoms were fixed in their calculated positions. Molecular structures were drawn using ORTEP[41].

**Syntheses of complexes**

**$[Me_2Sn(2\text{-}SC_5H_4N)_2]$ (1)**

To a freshly prepared methanolic solution of $NaSC_5H_4N$ [from methanolic solutions of 2-$HSC_5H_4N$ (161 mg, 1.45 mmol) and $NaOCH_3$ [78 mg (14.4 ml of 0.1 M), 1.44 mmol)], solid $Me_2SnCl_2$ (158 mg, 0.72 mmol) was added with vigorous stirring. The reaction mixture was stirred at room temperature for 2 h and the solvents were evaporated under vacuum. The residue was washed thoroughly with diethylether and the residue was extracted with chloroform and passed through a G3 filtration assembly to remove NaCl. The filtrate was dried under reduced pressure and the residue was recrystallized from methanol to yield pale yellow crystals of the title complex (Yield: 174 mg, 65%), mp 138 $^oC$. Anal. Calcd. for $C_{12}H_{14}N_2S_2Sn$: C, 39.05; H, 3.82; S, 17.38%. Found: C, 38.85; H, 3.75; S, 16.04%. $^1H$ NMR ($CDCl_3$) $\delta$: 1.01 (s, $Me_2Sn$, 6 H, $^2J$(Sn–H) = 75.9 Hz); 6.93 (t, C*H*-4, 2 H, 6.2 Hz); 7.30 (d, C*H*-3, 2 H, 7.8 Hz); 7.46 (t, C*H*-5, 2 H, 7.7 Hz); 8.07 (d, C*H*-6, 2 H, 4.2 Hz). $^{13}C\{^1H\}$ NMR

($CDCl_3$) $\delta$: 7.1 ($Me_2Sn$, $^1J(^{119}Sn\text{-}^{13}C)$ = 601 Hz; $^1J(^{117}Sn\text{-}^{13}C)$ = 575 Hz), 118.0 (C-4), 124.6 (C-5), 136.9 (C-3), 146.4 (C-6), 163.3 (C-S). $^{119}Sn\{^1H\}$ NMR ($CDCl_3$) $\delta$: −119 ppm.

**[$Et_2Sn(2\text{-}SC_5H_4N)_2$] (2)**

Prepared in a similar fashion to **1** and recrystallized from methanol as colorless crystals in 64% yield, mp 112°C. Anal. Calcd. for $C_{14}H_{18}N_2S_2Sn$: C, 42.34; H, 4.57; S, 16.15%. Found: C, 41.98; H, 4.45; S, 15.64%. $^1H$ NMR ($CDCl_3$) $\delta$: 1.29 (t, $SnCH_2CH_3$, 6 H, 7.8 Hz); 1.59 (m, $CH_2CH_3$, 4 H); 6.92 (t, C*H*-5, 2 H, 6.2 Hz); 7.30 (d, C*H*-3, 2 H, 8.1 Hz); 7.45 (d,t, C*H*-5, 2 H, 1.5 (d), 8.4 (t) Hz); 8.12 (d, C*H*-6, 2 H, 4.8 Hz). $^{13}C\{^1H\}$ NMR ($CDCl_3$) $\delta$: 10.4 ($SnCH_2CH_3$, $^2J(^{119}Sn\text{-}^{13}C)$ = 41 Hz), 19.1 ($SnCH_2$, $^1J(^{119}Sn\text{-}^{13}C)$ = 588 Hz; $^1J(^{117}Sn\text{-}^{13}C)$ = 560 Hz); 117.9 (C-4), 124.7 (C-5), 136.8 (C-3), 146.6 (C-6), 164.0 (C-S). $^{119}Sn\{^1H\}$ NMR ($CDCl_3$) $\delta$: −116 ppm.

**[$Et_2SnCl(2\text{-}C_5H_4N)$] (3)**

To a toluene solution of [$Et_2SnCl(2\text{-}C_5H_4N)_2$] (74 mg, 0.19 mmol) solid $Et_2SnCl_2$ (46 mg, 0.19 mmol) was added and the contents were stirred at room temperature for 1 hr. The solvent was evaporated under vacuum and the residue was washed with hexane and again dried to give cream colored sticky mass (yield 70% ). $^1H$ NMR ($CDCl_3$) $\delta$: 1.33 (t, $SnCH_2CH_3$, 7.8 Hz), 1.64 (m, $SnCH_2$), 7.05 (t, 6 Hz), 7.27 (d, 8.4 Hz), 7.59 (t, 8.1 Hz), 7.94 (d, 5.3 Hz). $^{13}C\{^1H\}$ NMR ($CDCl_3$) $\delta$: 10.0 ($SnCH_2CH_3$, $^2J$(Sn-C) = 38 Hz), 17.9 ($SnCH_2$, $^1J(^{119}Sn\text{-}^{13}C)$ = 529 Hz, $^1J(^{117}Sn\text{-}^{13}C)$ = 505 Hz), 119.0, 123.9, 138.9, 145.8, 164.7 ppm. $^{119}Sn\{^1H\}$ NMR ($CDCl_3$) $\delta$: −57 ppm.

**[$Me_2SnCl\{SC_4H(Me\text{-}4,6)_2N_2\}$] (4)**

To a freshly prepared methanolic solution of $NaSC_4H(Me\text{-}4,6)_2N_2$ [from methanolic solutions of $2\text{-}HSC_4H(Me\text{-}4,6)_2N_2$ (153 mg, 1.09 mmol) and $NaOCH_3$ [58 mg (10.9 ml of 0.1 M), 1.07 mmol)], solid $Me_2SnCl_2$ (119 mg, 0.54 mmol) was added with vigorous stirring which continued for 2 h. The solvents were removed under reduced pressure. The residue was washed thoroughly with diethylether and the residue was extracted with chloroform and filtered to remove NaCl. The filtrate was dried under vacuum to give a yellow solid which was recrystallized from methanol to yield pale yellow crystals of **4** (Yield: 158 mg, 67.5%), mp 102 °C. Anal. Calcd. for $C_8H_{13}ClN_2SSn$: C, 29.71; H, 4.05; S, 9.91%. Found: C, 29.32; H, 4.12; S, 10.35%. $^1H$ NMR ($CDCl_3$) $\delta$: 1.09 (s, $Me_2Sn$, 6 H, $^2J$(Sn–H) = 72 Hz); 2.36 (s, $C_4H(Me\text{-}4,6)N_2$, 6 H); 6.76 (s, C*H*-5, $C_4H(Me\text{-}4,6)N_2$). $^{13}C\{^1H\}$ NMR ($CDCl_3$) $\delta$: 5.7 ($SnCH_3$, $^1J(^{119}Sn\text{-}^{13}C)$ = 561 Hz; $^1J(^{117}Sn\text{-}^{13}C)$ = 536 Hz), 23.0 ($C_4H(Me\text{-}4,6)N_2$), 115.6 (C-5), 167.3 (C-4,6), 173.9 (C-S). $^{119}Sn\{^1H\}$ NMR ($CDCl_3$) $\delta$: −66 ppm.

**[$Et_2SnCl\{SC_4H(Me\text{-}4,6)_2N_2\}$] (5)**

Prepared in a similar fashion to **4** and recrystallized from methanol as pale yellow crystals in 66% yield, mp 126 °C. Anal. Calcd. for $C_{10}H_{17}ClN_2SSn$: C, 34.17; H, 4.88; S, 9.12%. Found: C, 34.59; H, 4.86; S, 9.80%. $^1H$ NMR ($CDCl_3$) $\delta$: 1.36 (t, $SnCH_2CH_3$, 6 H, 7.8 Hz); 1.63 (m, $CH_2CH_3$, 4 H); 2.35 (s,

$C_4H(Me\text{-}4,6)N_2$, 6 H); 6.75 (s, C*H*-5, $C_4H(Me\text{-}4,6)N_2$). $^{13}C\{^1H\}$ NMR ($CDCl_3$) $\delta$: 9.9 ($SnCH_2CH_3$, $^2J(^{119}Sn\text{-}^{13}C)$ = 41 Hz), 17.3 ($SnCH_2$, $^1J(^{119}Sn\text{-}^{13}C)$ = 522 Hz; $^1J(^{117}Sn\text{-}^{13}C)$ = 500 Hz), 23.3 ($C_4H(Me\text{-}4,6)N_2$), 115.5 (C-5), 167.2 (C-4,6), 174.5 (C-S). $^{119}Sn\{^1H\}$ NMR ($CDCl_3$) $\delta$: –58 ppm.

**Preparation of tin sulfide nanoparticles**

In a typical experiment, $[Et_2Sn(2\text{-}SC_5H_4N)_2]$ (**2**) (100 mg, 0.25 mmol) dispersed in OLA (2 ml) was injected rapidly into a preheated (300 $^oC$) OLA (8 ml) with vigorous stirring under flowing argon. The reaction mixture was held at this temperature for different durations (10 and 20 min). After the desired growth time, the reaction temperature was cooled down rapidly to 98 °C and quenched by injecting toluene (4 ml). The resulting nanocrystals were separated by precipitating with excess methanol followed by centrifugation to give a black powder. Similarly, $[Et_2SnCl\{SC_4H(Me\text{-}4,6)_2N_2\}]$ (**5**) (100 mg, 0.28 mmol) was thermolysed under same conditions (5 and 10 minutes). The **5** also was thermolysed in TOPO (3 g, 7.76 mmol)/OLA at 320 $^oC$ and the nanocrystals were isolated similarly.

## Results and discussion

### Synthesis and Spectroscopy

Treatment of $R_2SnCl_2$ (R = Me or Et) with two equivalents of sodium pyridyl/4,6-dimethyl-2-pyrimidyl thiolates, $NaSC_5H_4N$/ $NaSC_4H(Me\text{-}4,6)_2N_2$, in a toluene-methanol mixture gave diorganotin thiolate complexes of the type, $[R_2Sn(SC_5H_4N)_2]$ and $[R_2Sn\{SC_4H(Me\text{-}4,6)_2N_2\}Cl]$, respectively (Scheme 1).

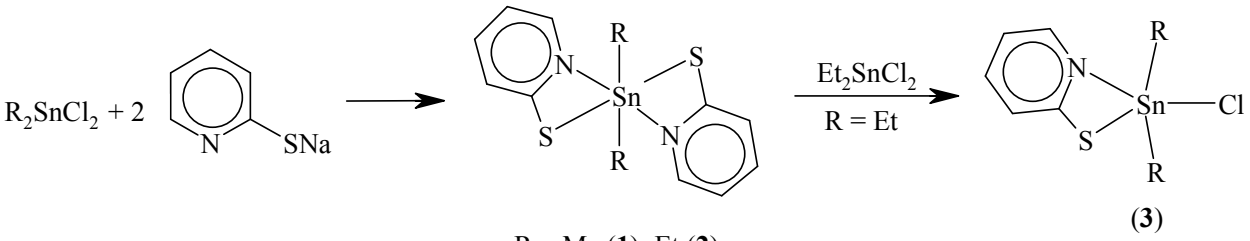


R = Me (**1**); Et (**2**)

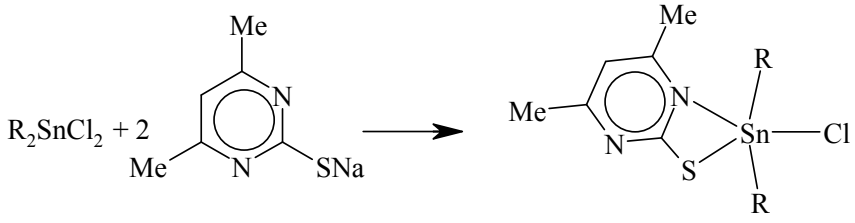


R = Me (**4**); Et (**5**)

**Scheme 1**

The $^{1}H$, $^{13}C\{^{1}H\}$ and $^{119}Sn\{^{1}H\}$ NMR spectra were recorded in $CDCl_3$ (Supplementary information Figs. S6-S14). $^{1}H$ and $^{13}C$ NMR spectra showed expected resonances and peak multiplicities. The pyridyl/ pyrimidyl ring proton resonances of all the complexes shifted to down field with reference to the corresponding signals for free ligand. There is an appreciable shift in the CH-6 proton resonances of the 2-pyridylthiolate complexes (**1** and **2**) with respect to its position in free ligand. This may be attributed to tin-nitrogen coordination resulting in chelation of the ligand. The CH-5 proton resonance for **4** and **5** is shielded with respect to the free ligand. The magnitude of $^{2}J(^{119}Sn–^{1}H)$ for **1** (~76 Hz) is smaller than expected for six coordinated dimethyltin complexes[42] while $^{2}J$(Sn-H) (~72 Hz) for **4** is in accordance with five coordinate dimethyltin complexes. The C–Sn–C angles for **1** and **4** have been estimated as 129° and 125°, respectively by Lockhart and Davidson's relationship [$^{1}J(^{119}Sn–^{13}C) = 10.7$ (∠C–Sn–C) –778)][43]. Similarly the magnitude of $^{1}J$(Sn-C) coupling constants for **1**-**5** are consistent with six (**1** and **2**) and five (**3**-**5**) coordinate diorganotin complexes[44]. The C–Sn–C values for **1** and **4** estimated from NMR can be compared with the one determined by X-ray structural analysis (125.1(5)[45] and 126.5(4)°, respectively) (see later) suggesting that the solid state structure is retained in solution. The C–Sn–C angle in octahedral diorganotin complexes varies from 110–180° depending on a skew to regular *trans* arrangement of R groups on central tin atom.[42]

The $^{119}Sn\{^{1}H\}$ NMR spectra showed single resonances in the range –57 to –119 ppm and these signals within the series (bis or chloro) are deshielded on replacing methyl groups on tin by Et groups which could be due to +I effect of the larger alkyl group. Similarly, $^{119}Sn$ NMR resonances for the complexes **1**-**5** are deshielded with respect to their selenium analogues as S is more electronegative than selenium which results in more deshielding. The difference in the chemical shift (~30 ppm) is more pronounced when R is methyl group. The $^{119}Sn$ NMR chemical shifts for **1**-**2** and **3**-**5** are lower than the ranges reported for six-coordinated (–125 to –400 ppm) and five-coordinated (–90 to –200 ppm) diorganotin complexes with O-bonded and halide ligands.[46] The deviation from the expected ranges may be attributed to the difference in the polarities of Sn-S and Sn-O bonds.[46]

**X-ray Crystallography**

The molecular structures of $[Et_2Sn(2\text{-}SC_5H_4N)_2]$ (**2**), $[Me_2SnCl\{SC_4H(Me\text{-}4,6)_2N_2\}]$ (**4**) and $[Et_2SnCl\{SC_4H(Me\text{-}4,6)_2N_2\}]$ (**5**) have been established by single crystal X-ray diffraction analysis. The selected inter-atomic parameters are given in tables 2-4 while ORTEP drawings with crystallographic numbering scheme are shown in Figs. 1-3. The Sn–C (2.11(2) – 2.199(8) Å ), Sn–S (~2.45 Å)[47,44] and Sn–Cl (~2.43 Å)[47,48] are well in agreement with those reported for diorganotin(IV) complexes[45,49,50].

The overall coordination environment around tin in **2** is similar to other analogous structures of $R_2Sn(Spy)_2$ (R = Me[45], Ph[51] and c-Hex [52]) which have a skew trapezoidal bipyramidal geometry. The N–Sn–N angle in **2** is compressed (145.85º) than the one found in $Me_2Sn(Spy)_2$ (152.1(2)º)[45] whereas the converse was noted for S–Sn–S angle (92.28(17)º in (**2**) vs 86.91(7)º in $[Me_2Sn(Spy)_2]$[45] and 89.9(1)° in $[Bu^n_2Sn\{SC_5H_3N(5\text{-}NO_2)\}_2]$[53].

The tin in $[R_2SnCl\{SC_4H(Me\text{-}4,6)_2N_2\}]$ (R = Me (**4**) and Et (**5**)) adopts a distorted trigonal bipyramidal configuration defined by $R_2$, N, S and Cl donors. The chloride and the chelating 2-mercapto dimethylpyrimidyl group occupy equatorial plane while the two organic groups are axially disposed. The Sn–N distances (~ 2.51 Å) are slightly longer than the one reported in $[Ph_2SnCl(Spy)]$ (2.413 Å)[47], but significantly shorter than bis thiopyridinates, $Me_2Sn(Spy)_2$ (2.702(5) Å)[45].

**Thermal studies**

Thermo gravimetric analyses (TGA) (Supplementary information, Fig.s S1-S4) of these complexes were carried out under a flowing argon atmosphere. The complexes, $[R_2Sn(2\text{-}SC_5H_4N)_2]$ (R = Me or Et) undergo a single-step decomposition leading to the formation of $SnS_2$ (weight loss: found 72.3%, calcd. 75.2% for $[Me_2Sn(2\text{-}SC5H_4N)_2]$ (**1**); and found 78.2%, calcd. 76.9% for $[Et_2Sn(2\text{-}SC_5H_4N)_2]$ (**2**)).

The complexes, $[R_2SnCl\{SC_4H(Me\text{-}4,6)_2N_2\}]$ (R = Me (**4**) or Et (**5**)) decompose in a single step at 200 °C for **4** and 288 °C for **5**. The weight loss was significantly higher for the complexes than expected for either formation of $SnS_2$/SnS. It is likely that the complexes undergo disproportionation into $R_2SnCl_2$ and $R_2Sn\{SC_4H(Me\text{-}4,6)_2N_2\}_2$ and the former vaporizes while latter decomposes to stable tin sulfide. To ascertain disproportionation, **5** was sublimed under vacuum. The complex sublimed with decomposition. Yellow sublimate showed two $^{119}$Sn NMR resonances at δ −56.2 and −111.7 ppm attributable to **5** and $[Et_2Sn\{SC_4H(Me\text{-}4,6)_2N_2\}_2]$, respectively (Supplementary information, Fig. S5).

**Preparation and characterization of tin sulfide nanostructures**

The TG data indicate that these complexes decompose to tin sulfide, thus two representative diethyltin complexes were chosen to assess their suitability of single source molecular precursor for tin sulfide. Tin sulfide nanostructures were prepared by employing **2** and **5**. The resulting products were characterized by solid state diffuse reflectance, FT-IR, thermo gravimetric analysis, X-ray powder diffraction (XRD), energy dispersive X-ray analysis (EDX) (Supplementary information), SEM, TEM and selective area electron diffraction (SAED) techniques.

**Preparation of tin sulfide nanostructures**

Tin sulfide nanostructures were prepared by injecting diethyltin complexes, **2** and **5,** in high boiling coordinating solvents like OLA or TOPO. Initially, the use of OLA as surface passivating agent (surfactant) to prepare tin sulfide nanostructures was driven by the fact that amines have good affinity for tin and secondly, ease of handing OLA during the purification of nanocrystals. However, the average size of nanostructures as calculated by Scherrer's formula comes out to be in the range of 30.9-39.7 nm (see later PXRD discussion in "characterization of tin sulfide nanostructures). So, in order to achieve the nanostructures of smaller size, either reaction timing or the injection temperature may be reduced or strong coordinating ligand like TOPO can be used as a surfactant. However, reduction either in the injection temperature below 300 $^{o}$C or the reaction time less than 5 minutes resulted in incomplete decomposition. Thus, TOPO was used as surfactant for thermolysis of **5** to prepare smaller nanostructures of tin sulfide. The initial pale yellow solution of the complex turned dark yellow on thermolysis in TOPO-OLA which gradually changed to red and dark brown from which tin sulfide nanoparticles were separated and characterized.

**Characterization of tin sulfide nanostructures**

Thermolysis of **2** (0.25 mmol) and **5** (0.28 mmol) in OLA for different duration (experimental section) at 300 $^{o}$C gave black residue of tin sulfide. The crystal structure and phase purity of the black residues was investigated using powder X-ray diffraction (PXRD) technique. The XRD pattern of the residue obtained by thermolysis of **2** in OLA at 300 $^{o}$C for 10 minutes exhibited peaks at 22.0, 25.9, 27.4, 30.5, 31.6, 32.0, 39.0, 42.5, 44.6, 45.5, 48.7, 51.3, 52.1, 53.4, 54.2, 56.6 and 59.5$^{o}$. These peaks can be assigned to the reflections originating from (110), (120), (021), (101), (130), (040), (131), (210), (141), (002), (060), (151), (032), (160), (061), (132) and (250) planes of orthorhombic SnS (JCPDS-39-0354) (Figure 4b, Supplementary Fig. S18). The lattice parameters for these nano-structures determined from the PXRD data using equation 1 (where h, k, and l are the lattice planes while a, b, c are lattice parameters and d is the inter-planar distance) are a = 4.340(13) Å, b = 11.191(20) Å, c = 3.984(10) Å, which are consistent with literature values (a = 4.329 Å, b = 11.19 Å, c = 3.983 Å) for orthorhombic SnS (JCPDS-39-0354). The intensity of these Brag reflections indicates their crystalline nature. The average crystallite size as estimated by Scherrer's formula is 38 nm. Its composition is supported by EDX (from **2**, Sn:S atom ratio is 53.8:46.2 or 1.2:1) (Figure 5b).

$$\frac{1}{d^2} = \frac{h^2}{a^2} + \frac{k^2}{b^2} + \frac{l^2}{c^2} \qquad \text{.....(1)}$$

Similarly, XRD profile of the residue obtained by thermolysis of **5** in OLA at 300 $^{o}$C for 5 and 10 minutes showed peaks and their intensities corresponding to orthorhombic SnS (JCPDS-39-0354) (Figure 4c and 4d, Supplementary Fig. S19). The composition is supported by EDX analysis (from **5**: Sn:S atom ratio is 52:48 or 1.1:1 (for 5 minutes); Sn:S atom ratio is 54.3:45.6 or 1.2:0.8 (for 10 minutes)). The lattice parameters for these residues are a = 4.326(2) Å, b = 11.217(3) Å, c = 3.982(3) (for 5 min.) and a = 4.328(8) Å, b = 11.194(1) Å, c = 3.990(7) (for 10 min.), respectively which are in accord with the orthorhombic SnS (JCPDS-39-0354). Scherrer analysis of the intense reflection gave the average grain sizes of the two residues as 30.9 and 39.7 nm, respectively.

The SEM micrographs showed that the residues obtained by thermolysis of **2** and **5** have hexagonal and nearly rectangular sheet structures, respectively (Figure 5a and 5b). For instance, thermolysis of **2** afforded hexagonal sheets having edges of few microns while thermolysis of **5** gave nearly rectangular sheets with length and breadth of few hundred nanometers with thickness of 30-80 nm (majority being in the range of 35-60 nm). TEM images of tin sulfides (Figures 6a and 7a) prepared by thermolysis of **2** and **5** in OLA showed hexagonal sheets (edges in the range of 200-350 nm) and a rectangular sheet (width of 310 nm, length of 390 and thickness of 58 nm), respectively. The SAED patterns (Figures 6b and 7b) exhibited dot like pattern with sets of lattice planes, (040), (023), (063) (from **2**) and (041), (200), (241) (from **5**) related to orthorhombic SnS (JCPDS-39-0354) and were consistent with the XRD results. The dots like patterns suggest that SnS sheets are single crystalline in nature.

Unlike thermolysis in olylamine, the decomposition in TOPO-OLA gave a mixture of tin sulfides (SnS and $SnS_2$), although the size of the resulting nanoparticles was smaller (by PXRD). The average size estimated from Scherrer's formula is 16.5 nm from thermolysis of **5** (Supporting information Figure S15). The morphologies of tin sulfides obtained by thermolysis of **5** in TOPO-OLA showed square shaped sheets (edge of 49-127 nm) contaminated with nearly spherical structures (diameter 42 nm) (Figure 8a). SAED pattern of square shaped sheets showed lattice fringes, (130), (121), (251) (square sheets) corresponds to orthorhombic of SnS (JCPDS-39-0354) (Figure 8b).

**Surface properties of the nanostructures**

Since the thermolysis in olylamine gave phase pure single composition of tin sulfide, further investigations were carried out on these samples. The surface characterization of tin sulfide nanostructures was studied by employing FT-IR spectroscopy (Supporting information Figure S16) and thermo gravimetric analysis (Supporting information Figure S17). FTIR spectra of SnS nano structures obtained by thermolysis of **2** and **5** showed different characteristic IR modes corresponding to $\nu_{N-H}$ (3303–3308 $cm^{-1}$), $\nu_{CH2}$ (anti-symmetric 2914 $cm^{-1}$ and symmetric 2850 $cm^{-1}$) stretches, $\delta_{N-H}$ bending mode (1531-1546$cm^{-1}$)[54] indicating the presence of alkyl amines. The $\nu_{N-H}$ stretches are broad which is

generally observed for the nanostructures capped by amine ligands such as OLA. Both $\nu_{N-H}$ and $\delta_{N-H}$ bands are shifted to lower wave numbers with respect to the amine group of free OLA ($\nu_{N-H}$ = 3373cm$^{-1}$ and $\delta_{N-H}$= 1561cm$^{-1}$ [54]) suggesting –$NH_2$ is bound to the surface of nanostructures. Thermo gravimetric analyses of the latter confirm the presence of amines on their surface.

Thermo gravimetric profile of the nanostructures synthesized in OLA showed overlapping step decomposition leading to an overall weight loss of ~17% when the temperature is increased step-wise from room temperature to 800 $^{o}$C. The differential curve of TGA displayed three peaks (a prominent and two small) consistent with decomposition steps at 189, 321 and 418 °C (Figure S16). The first step involving a small weight loss of 2.9% below 189 $^{o}$C may be attributed to the removal of crystalline and adsorbed water on the surface of the nanostructures[55]. After the first step, a gradual and slow thermal decomposition is observed in the temperature range of 200-600 $^{o}$C which may be accounted for the loss of capping ligands (OLA). Such type of a gradual loss was also observed OLA capped $Cu_2ZnSnS_4$ nanocrystals and was attributed to the long alkyl chains of OLA.[56] Different IR modes of FTIR spectra corroborated by thermo gravimetric analysis confirm the existence of OLA on the surface of the nanostructures.

**Optical properties of SnS nanostructures**

Optical properties of the tin sulfide nanostructures were studied using solid state diffuse reflectance spectroscopy. To determine the optical direct and indirect band gaps, Kubeka-Munk transformations were carried out on solid state diffuse reflectance data. The plots of $[F(R)h\nu]^2$ versus $h\nu$ and $[F(R)h\nu]^{1/2}$ versus $h\nu$ were used to obtain direct and indirect band gaps, respectively (Figure 9). The band gaps were measured by extrapolating the linear portion of the plot to X (energy) axis. The direct gap estimated for hexagonal sheets (from **2**) is 1.62 eV while the values for that of rectangular sheets (from **5**) are 1.90 (5 minutes) and 1.6 (10 minutes) eV. However, the indirect band gaps for all the samples are nearly 1.46 eV. The direct and indirect band gaps are blue shifted with respect to bulk SnS [$E_g$ (direct) = 1.3 eV and $E_g$ (indirect) = 1.1 eV)] to the tune of 0.3-0.6 eV and 0.36 eV, respectively. The thicknesses of both the hexagonal and rectangular sheets are larger than the Bohr radius reported for bulk SnS (7 nm) and hence the blue shift in the direct band gaps cannot be accounted for quantum size effects. The increased band gaps may be attributed to the surface effect of the carriers, lattice distortions or surface lattice defects.[57]

**Conclusions**

Diorganotin(IV) pyridyl- and pyrimidyl thiolates have been synthesized and isolated as air stable monomeric complexes. Diorganotin(IV) thiolate complexes have been utilized as single source precursors

for the preparation of phase pure tin sulfide nano-sheets. Hexagonal and rectangular sheets were isolated by thermolysis of different precursors. The thickness of the sheets are in the range of 30-80 nm which showed direct and indirect band gaps spanning from 1.6-1.9 eV and 1.46 eV, respectively. A shift of 0.31-0.6 eV with respect to bulk band gaps can be accounted for the surface effect of the carriers, lattice distortions or surface lattice defects.

**Acknowledgements**

We thank Dr. B. N. Jagatap for encouragement of this work. We are grateful to Head, Analytical Chemistry Division and (Mrs.) N. Raje for providing thermo gravimetric analyses data.

**Supporting Information**

CCDC-Nos. 1063157 (**2**), 1063159 (**4**) and 1063158 (**5**) for $[Me_2Sn(2\text{-}SC_5H_4N)_2]$ (**1**), $[Me_2SnCl\{SC_4H(Me\text{-}4,6)_2N_2\}]$ (**4**) and $[Et_2SnCl\{SC_4H(Me\text{-}4,6)_2N_2\}]$ (**5**), respectively contain the supplementary crystallographic data for this paper. These data can be obtained free of charge at www.ccdc.cam.ac.uk/conts/retrieving.html or from the Cambridge Crystallographic Data Centre, 12 Union Road, Cambridge CB2 1EZ, UK [Fax: + 44-1223/336-033; E-mail: deposit@ccdc.cam.ac.uk].

## References

1. M. A. Franzman, C. W. Schlenker, M. E. Thompson and R. L. Brutchey, *J. Am. Chem. Soc.*, 2010, **132**, 4060.
2. N. R. Mathews, *Solar Energy*, 2012, **86**, 1010.
3. L. -D. Zhao, S. -H. Lo, Y. Zhang, H. Sun, G. Tan, C. Uher, C. Wolverton, V. P. Dravid and M. G. Kanatzidis, *Nature*, 2014, **508**, 373-378.
4. G. Kedarnath, L. B. Kumbhare, S. Dey, A. P. Wadawale, V. K. Jain and G. K. Dey, *Polyhedron*, 2009, **28**, 2749.
5. N. Wang, X. Cao, L. Guo, S. Yang and Z. Wu, *ACS Nano*, 2 (2008) 184–190.
6. M. C. Weidman, M. E. Beck, R. S. Hoffman, F. Prins and W. A. Tisdale, *ACS Nano*, 2014, **8**, 6363.
7. Z. Quan, W. S. Loc, C. Lin, Z. Luo, K. Yang, Y. Wang, H. Wang, Z. Wang and J. Fang, *Nano Lett.*, 12 (2012) 4409–4413.
8. T. Mandal, G. Piburn, V. Stavila, I. Rusakova, T. Ould-Ely, A. C. Colson, and K. H. Whitmire, *Chem. Mater.*, 2011, **23**, 4158.

9. D. Zhang, G. Zhai, J. Zhang, L. Yuan, X. Miao, S. Zhu and Y. Wang, *Cryst. Eng. Comm.*, 2010, **12**, 3243.
10. M. A. Sliem, A. Chemseddine, U. Bloeck and R. A. Fischer, *Cryst. Eng. Comm.*, 2011, **13**, 483.
11. M. Shi, W. Su and H. Matsui, *Nanoscale*, 2010, **2**, 2373.
12. T. Jiang and G. A. Ozin, *J. Mater. Chem.*, 1998, **8**, 1099.
13. J. P. Singh and R. K. Bedi, *Thin Solid Films*, 1991, **199,** 9.
14. M. Parenteau and C. Carlone, *Phys. Rev. B*, 1990, **41**, 5227.
15. P. Pramanik, P. K. Basu and S. Biswas, *Thin Solid Films*, 1987, **150**, 269.
16. J. B. Johnson, H. Jones, B. S. Lathan, J. D. Parker, R. D. Engelken and C. Barber, *Semicond. Sci. Technol.*, 1999, **14**, 501.
17. M. Radot, *Rev. Phys. Appl.*, 1977, **18**, 345.
18. M. Devika, K. T. Ramakrishna Reddy, N. Koteeswara Reddy, K. Ramesh, R. Ganesan, E. S. R. Gopal and K. R. Gunasekhar, *J. Appl. Phys.*, 2006, **100**, 023518.
19. E. C. Greyson, J. E. Barton and T. W. Odom, *Small*, 2006, **2**, 368.
20. S. G. Hickey, C. Waurisch, B. Rellinghaus and A. Eychmuller, *J. Am. Chem. Soc.*, 2008, **130**, 14978.
21. Z. Deng, D. Han and Y. Liu, *Nanoscale*, 2011, **3**, 4346.
22. J. Ning, K. Men, G. Xiao, L. Wang, Q. Dai, B. Zou, B. Liu and G. Zou, *Nanoscale*, 2010, **2**, 1699.
23. H. Liu, Y. Liu, Z. Wang and P. He, *Nanotechnology*, 2010, **21**, 105707.
24. H. Zhang, B. -R. Hyun, F. W. Wise and R. D. Robinson, *Nano Lett.*, 2012, **12**, 5856.
25. Deng, D. Cao, J. He, S. Lin, S. M. Lindsay and Y. Liu, *ACS Nano*, 2012, **6**, 6197.
26. T. G. Hibbert, M. F. Mahon, K. C. Molloy, L. S. Price and I. P. Parkin, *J. Mater. Chem.*, 2001, **11**, 464.
27. L. S. Price, I. P. Parkin, T. G. Hibbert and K. C. Molloy, *Chem. Vap. Deposition*, 1998, **4**, 222.
28. A. Sanchhez-Juarez, A. Tiburcio-Silver and A. Oritz, *Thin Solid Films*, 2005, **480**, 452.
29. B. P. Bade, S. S. Garje, Y. S. Niwate, M. Afzaal and P. O'Brien, *Chem. Vap. Deposition*, 2008, **14**, 292.
30. A. Abou Sharma and H. M. Zeyada, *Opt. Mater.*, 24 (2003) 555.
31. S. K. Arora, D. H. Patel and M. K. Agarwal, *J. Mater. Sci.*, 1994, **29**, 3979.
32. P. Sinsermsuksakul, J. Heo, W. Noh, A. S. Hock and R. G. Gordon, *Adv. Energy Mater.*, 2011, **1**, 1116.
33. A. Goossens and J. Schoonman, *Eur. J. Solid State Inorg. Chem.*, 1995, **32**, 779.

34. K. Ramasamy, V. L. Kuznetsov, K. Gopal, M. A. Malik, J. Raftery, P. P. Edwards, and P. O'Brien, *Chem. Mater.*, 2013, **25**, 266.
35. D. S. Koktysh, J. R. McBride and S. J. Rosenthal, *Nanoscale Res. Lett.*, 2007, **2**, 144.
36. Y. Zhang, J. Lu, S. Shen, H. Xu and Q. Wang, *Chem. Commun.*, 2011, **47**, 5226.
37. S. C. Nigam, G. S. Saharia and H. R. Sharma, *J. Indian Chem. Soc.*, 1983, **60**, 583.
38. B. Philips-Invernizzi, D. Dupont, and C. Caze, *Opt. Eng.*, 2001, **40**, 1082.
39. T. Higashi, ABSCOR-Empirical Absorption Correction based on Fourier Series Approximation, Rigaku Corporation, 3-9-12 Matsubara, Akishima, Japan, 1995.
40. G. M. Sheldrick, SHELX 97-Program for Crystal Structure Analysis, Göttingen, Germany, 1997; Sheldrick, G. M. *Acta. Crystallogr. A*, 2008, **64**, 112.
41. C. K. Johnson, ORTEP II, Report ORNL-5136, Oak Ridge National Laboratory, Oak Ridge TN, 1976.
42. Charu Vatsa, Ph. D. Thesis, *University of Mumbai*, 1990.
43. T. P. Lockhart and F. Davidson, *Organomettalics*, 1987, **6**, 2471.
44. T. P. Lockhart, W. T. Manders and E. M. Holt, *J. Am. Chem. Soc.*, 1986, **108**, 6611.
45. M. V. Castaño, A. Macías, A. Castiñeiras, A. S. González, E. G. Martínez, J. S. Casas, J. Sordo, W. Hiller and E. E. Castellano, *J. Chem. Soc., Dalton Trans.*, 1990, 1001.
46. R. Schmiedgen, F. Huber, H. Preut, G. Ruisi and R. Barbieri, *Appl. Oranomet. Chem.*, 1994, **8**, 397.
47. R. Schmiedgen, F. Huber, H. Preut, G. Ruisi and R. Barbieri, *Appl. Organomet. Chem.*, 1994, **8**, 397.
48. S. D. Reid, A. L. Hector, W. Levason, G. Reid, B. J. Waller and M. Webster, *Dalton Trans.*, 2007, 4769.
49. E. O. Schlemper, *Inorg. Chem.*, 1967, **6**, 2012.
50. R. K. Sharma, G. Kedarnath, Amey Wadawale, C. A. Betty, B. Vishwanadh and V. K. Jain, *Dalton Trans.*, 2012, **41**, 12129.
51. R. Schmiedgen, F. Huber and H. Preut, *Acta Cryst. C*, 1993, **49**, 1735.
52. M. Bouâlam, J. Meunier-Piret, M. Biesemans, R. Willem and M. Gielen, *Inorg. Chim. Acta*, 1992, **198**, 249.
53. G. Domazetis, B. D. James, M. F. Mackay and R. J. Magee, *J. Inorg. Nucl. Chem.*, 1979, **41**, 1555.
54. O. Chen, Y. Yang, T. Wang, H. Wu, C. Niu, J. Yang and Y. C. Cao, J. *Am. Chem. Soc.*, 2011, **133**, 17504.

55. L. Ding, S. He, S. Miao, M. R. Jorgensen, S. Leubner, C. Yan, S. G. Hickey, A. Eychmüller, J. Xu and O. G. Schmidt, Nature, 2014, DOI: 10.1038/srep04647.

56. Y. Kim, K. Woo, I. Kim, Y. S. Cho, S. Jeong and J. Moon, *Nanoscale*, 2013, **5**, 10183

57. M. X. Wang, G. H. Yue1, Y. D. Lin, X. Wen, D. L. Peng and Z. R. Geng, *Nano-Micro Lett.*, 2013, **5**, 1.

Table 1. Crystallographic and structural determination data for $[Et_2Sn(2\text{-}SC_5H_4N)_2]$ (**2**), $[Me_2SnCl\{SC_4H(Me\text{-}4,6)_2N_2\}]$ (**4**) and $[Et_2SnCl\{SC_4H(Me\text{-}4,6)_2N_2\}]$ (**5**).

| | $[Et_2Sn(2\text{-}SC_5H_4N)_2]$ (**2**) | $[Me_2Sn\{SC_4H(Me\text{-}4,6)_2N_2\}Cl]$ (**4**) | $[Et_2Sn\{SC_4H(Me\text{-}4,6)_2N_2\}Cl]$ (**5**) |
|---|---|---|---|
| Chemical formula | $C_{14}H_{18}N_2S_2Sn$ | $C_8H_{13}ClN_2SSn$ | $C_{10}H_{17}ClN_2SSn$ |
| Formula weight | 397.11 | 323.42 | 351.45 |
| Crystal size/mm$^3$ | 0.10 × 0.10× 0.05 | 0.20 × 0.10× 0.01 | 0.15× 0.15 × 0.05 |
| Crystal system / space group | Orthorhombic/ P*nma* | Orthorhombic/ C*mca* | Monoclinic/ $P2_{1/n}$ |
| Unit cell dimensions | | | |
| a/Å | 9.9262(13) | 8.0000(10) | 10.6207(15) |
| b/Å | 17.2292(9) | 20.119(4) | 11.907(5) |
| c/Å | 9.7256(8) | 16.731(2) | 11.589(2) |
| α | 90.00 | 90.00 | 90.00 |
| β | 90.00 | 90.00 | 91.786(13) |
| γ | 90.00 | 90.00 | 90.00 |
| Volume/Å$^3$ | 1663.3(3) | 2692.9(7) | 1464.9(7) |
| Z | 4 | 8 | 4 |
| $D_c$/g cm$^{-3}$ | 1.586 | 1.595 | 1.594 |
| μ/mm$^{-1}$ | 14.467 | 2.216 | 2.044 |
| *F*(000) | 792 | 1264 | 696 |
| Limiting indices | $-6 \le h \le 11$ | $-9 \le h \le 5$ | $-7 \le h \le 13$ |
| | $-19 \le k \le 20$ | $-26 \le k \le 0$ | $-15 \le k \le 15$ |
| | $-11 \le l \le 11$ | $-12 \le l \le 21$ | $-15 \le l \le 15$ |
| No. of reflections collected / unique | 1587/ 920 | 1571/814 | 3364/1534 |
| No. of data / restraints / parameters | 1587/ 9/95 | 1571/0/79 | 3364/0/ 140 |
| Final $R_1$, $\omega R_2$ indices $[I > 2\sigma(I)]$ | 0.0706, 0.2017 | 0.0546, 0.1033 | 0.0538, 0.1120 |
| $R_1$, $\omega R_2$ (all data) | 0.1017, 0.2518 | 0.1411, 0.1280 | 0.1392, 0.1365 |
| Goodness of fit on $F^2$ | 1.091 | 0.976 | 0.990 |

Table 2. Selected bond lengths (Å) and angles (°) for $[Et_2Sn(2\text{-}SC_5H_4N)_2]$ (**2**)

| | | | |
|---|---|---|---|
| Sn1– S1 | 2.490(3) | Sn1– C8 | 2.11(2) |
| Sn1– S1$^{i}$ | 2.490(4) | Sn1– N1 | 2.661(10) |
| Sn1– C6 | 2.19(3) | S1– C1 | 1.753(14) |
| | | | |
| C6– Sn1–C8 | 145.6(13) | S1–Sn1– N1 | 60.9(3) |
| C6–Sn1–S1 | 99.5(8) | S1$^{i}$–Sn1– N1 | 153.2(3) |
| C6–Sn1–S1$^{i}$ | 99.5(8) | N1–Sn1– N1$^{i}$ | 145.88 |
| C8–Sn1–S1 | 104.1(4) | C1– S1– Sn1 | 88.8(5) |
| C8–Sn1– S1$^{i}$ | 104.1(4) | C1$^{i}$– S1$^{i}$– Sn1 | 88.8(5) |
| S1–Sn1– S1$^{i}$ | 92.28(17) | | |

Table 3. Bond lengths (Å) and angles (°) for $[Me_2SnCl\{SC_4H(Me\text{-}4,6)_2N_2\}]$ (**4**)

| | | | |
|---|---|---|---|
| Sn1–S1 | 2.443(3) | Sn1– Cl1 | 2.436(3) |
| Sn1–C7 | 2.199(8) | S1– C1 | 1.756(11) |
| Sn1– N1 | 2.505(8) | | |
| | | | |
| C7–Sn1– C7$^{i}$ | 126.5(4) | Cl1– Sn1– S1 | 91.87(10) |
| C7–Sn1– Cl1 | 100.4(2) | Cl1– Sn1– N1 | 155.3(2) |
| C7–Sn1– N1 | 90.5(2) | S1– Sn1– N1 | 63.4(2) |
| C7–Sn1– S1 | 114.0(2) | | |

Table 4. Bond lengths (Å) and angles (°) for $[Et_2SnCl\{SC_4H(Me\text{-}4,6)_2N_2\}]$ (**5**)

| | | | |
|---|---|---|---|
| Sn1–C7 | 2.120(9) | Sn1–S1 | 2.452(2) |
| Sn1–C9 | 2.123(9) | Sn1–N1 | 2.525(5) |
| Sn1–Cl1 | 2.438 (2) | S1–C1 | 1.740(8) |
| | | | |
| C7–Sn1–C9 | 128.0(4) | Cl1–Sn1–S1 | 91.48(9) |
| C7–Sn1–Cl1 | 101.7(3) | Cl1–Sn1–N1 | 154.60(17) |
| C7–Sn1–S1 | 112.5(3) | S1–Sn1–N1 | 63.15(16) |
| C7–Sn1–N1 | 90.0(3) | N1–C1–S1 | 114.4 (6) |
| C9–Sn1–Cl1 | 98.7(3) | Sn1–S1–C1 | 87.9(3) |
| C9–Sn1–S1 | 114.1(2) | Sn1–N1–C1 | 94.4(4) |
| C9–Sn1–N1 | 91.4(3) | | |

## Figure Captions

**Fig. 1** Crystal structure of $[Et_2Sn(2\text{-}SC_5H_4N)_2]$ (**2**) with atomic number scheme. The ellipsoids were drawn at 50% probability (H atoms are omitted for clarity).

**Fig. 2** Crystal structure of $[Me_2SnCl\{SC_4H(Me\text{-}4,6)_2N_2\}]$ (**4**) with atomic number scheme. The ellipsoids were drawn at 50% probability (H atoms are omitted for clarity).

**Fig. 3** Crystal structure of $[Et_2SnCl\{SC_4H(Me\text{-}4,6)_2N_2\}]$ (**5**) with atomic number scheme. The ellipsoids were drawn at 50% probability (H atoms are omitted for clarity).

**Fig. 4** a) Simulated XRD pattern of orthorhombic SnS (JCPDS-39-0354). XRD profiles of SnS nanosheets obtained by b) thermolysis of $[Et_2Sn(2\text{-}SC_5H_4N)_2]$ (**2**) in OLA at 300 $^oC$ for 10 minutes and by thermolysis of $[Et_2SnCl\{SC_4H(Me\text{-}4,6)_2N_2\}]$ (**5**) in OLA at 300 $^oC$ for c) 5 and d) 10 minutes, respectively.

**Fig. 5** SEM of SnS hexagonal and rectangular sheets obtained by thermolysis of $[Et_2Sn(2\text{-}SC_5H_4N)_2]$ (**2**) and $[Et_2SnCl\{SC_4H(Me\text{-}4,6)_2N_2\}]$ (**5**) in OLA at 300 $^oC$ for 10 and 5 minutes, respectively.

**Fig. 6** a) TEM image and b) SAED pattern of hexagonal SnS nanosheets prepared by thermolysis of $[Et_2Sn(2\text{-}SC_5H_4N)_2]$ (**2**) in OLA at 300 $^oC$ for 10 minutes.

**Fig. 7** a) TEM image and b) SAED pattern of rectangular SnS nanosheets prepared by thermolysis of $[Et_2SnCl\{SC_4H(Me\text{-}4,6)_2N_2\}]$ (**5**) in OLA at 300 $^oC$ for 5 minutes.

**Fig. 8** a) TEM image and b) SAED pattern of SnS nanosheets prepared by thermolysis of $[Et_2SnCl\{SC_4H(Me\text{-}4,6)_2N_2\}]$ (**5**) in TOPO-OLA at 320 $^oC$.

**Fig. 9** a) Solid-state diffuse reflectance spectrum of SnS rectangular sheets obtained by thermolysis of $[Et_2SnCl\{SC_4H(Me\text{-}4,6)_2N_2\}]$ (**5**) in OLA at 300 $^oC$ for 5 minutes and their Kubelka-Munk conversion plots of b) $[F(R)h\nu]^2$ vs energy and c) $[F(R)h\nu]^{1/2}$ vs energy from which direct and indirect band gaps were determined.

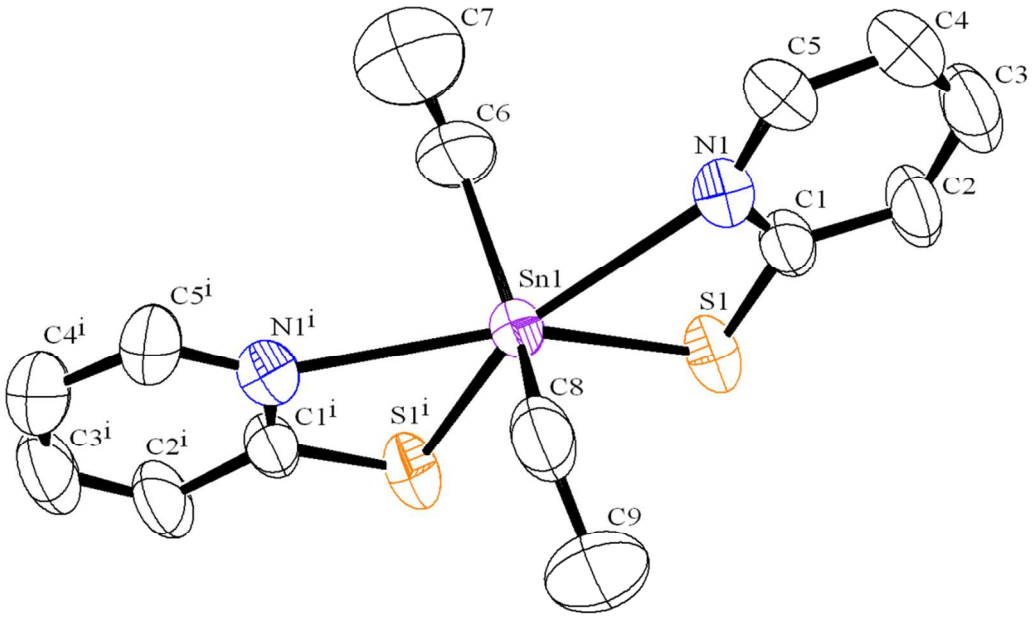


**Fig. 1** Crystal structure of $[Et_2Sn(2\text{-}SC_5H_4N)_2]$ (**2**) with atomic number scheme. The ellipsoids were drawn at 50% probability (H atoms are omitted for clarity).

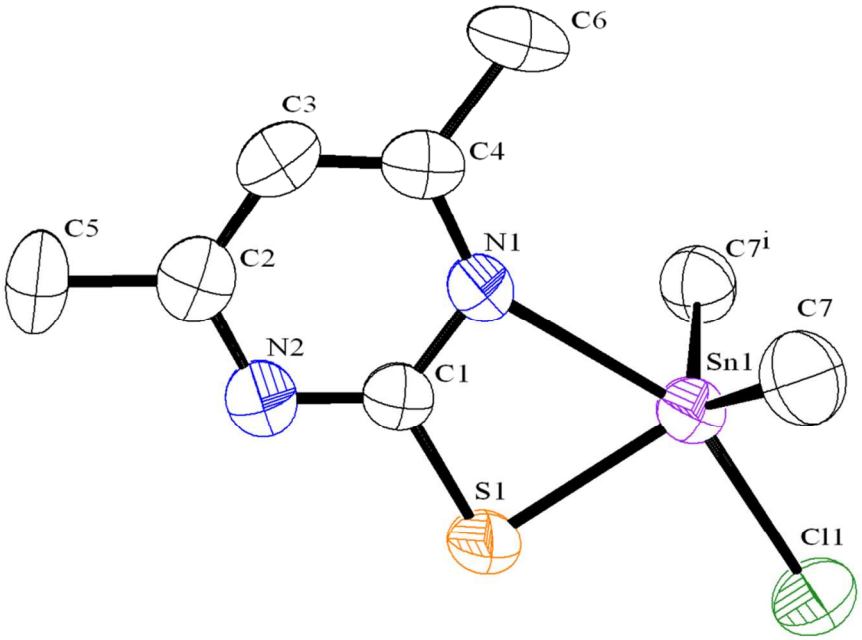


**Fig. 2** Crystal structure of $[Me_2SnCl\{SC_4H(Me\text{-}4,6)_2N_2\}]$ (**4**) with atomic number scheme. The ellipsoids were drawn at 50% probability (H atoms are omitted for clarity).

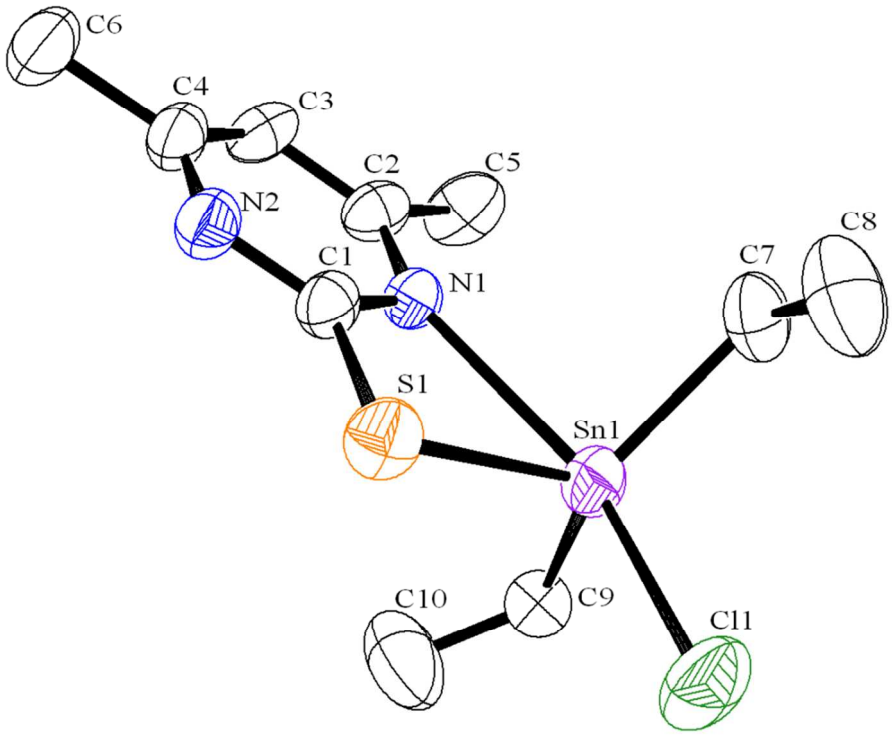


**Fig. 3** Crystal structure of $[Et_2SnCl\{SC_4H(Me\text{-}4,6)_2N_2\}]$ (**5**) with atomic number scheme. The ellipsoids were drawn at 50% probability (H atoms are omitted for clarity).

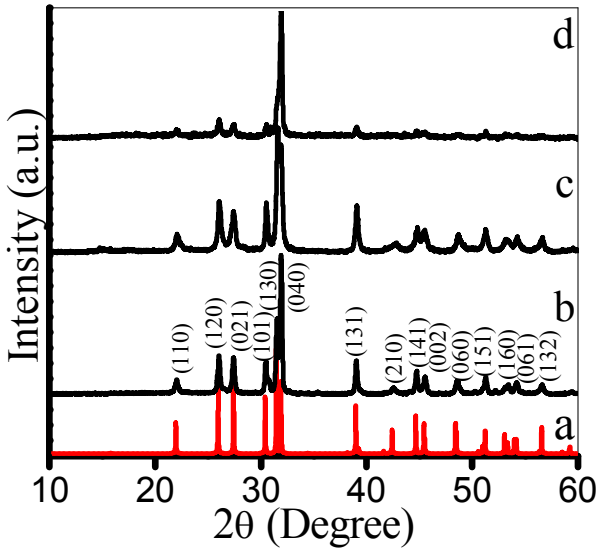


**Fig. 4** a) Simulated XRD pattern of orthorhombic SnS (JCPDS-39-0354). XRD profiles of SnS nanosheets obtained by b) thermolysis of $[Et_2Sn(2\text{-}SC_5H_4N)_2]$ (**2**) in OLA at 300 $^oC$ for 10 minutes and by thermolysis of $[Et_2SnCl\{SC_4H(Me\text{-}4,6)_2N_2\}]$ (**5**) in OLA at 300 $^oC$ for c) 5 and d) 10 minutes.

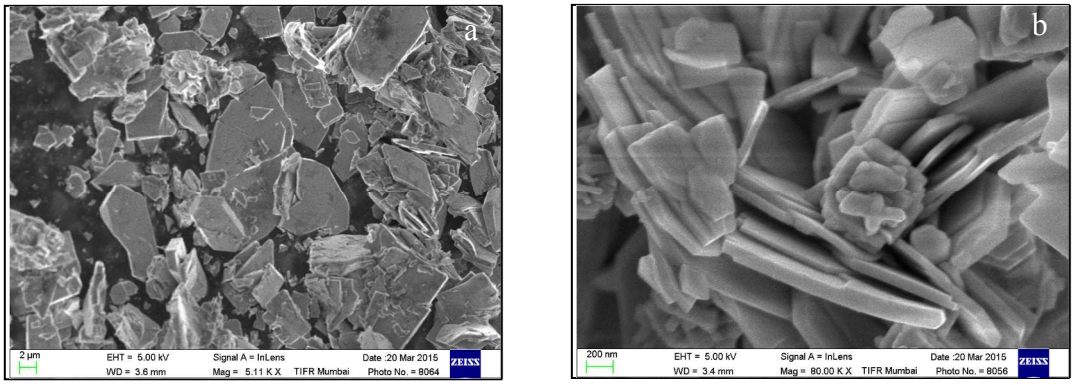


**Fig. 5** SEM images of SnS hexagonal and rectangular sheets obtained by thermolysis of a) $[Et_2Sn(2\text{-}SC_5H_4N)_2]$ (**2**) and b) $[Et_2SnCl\{SC_4H(Me\text{-}4,6)_2N_2\}]$ (**5**) in OLA at 300 $^oC$ for 10 and 5 minutes, respectively.

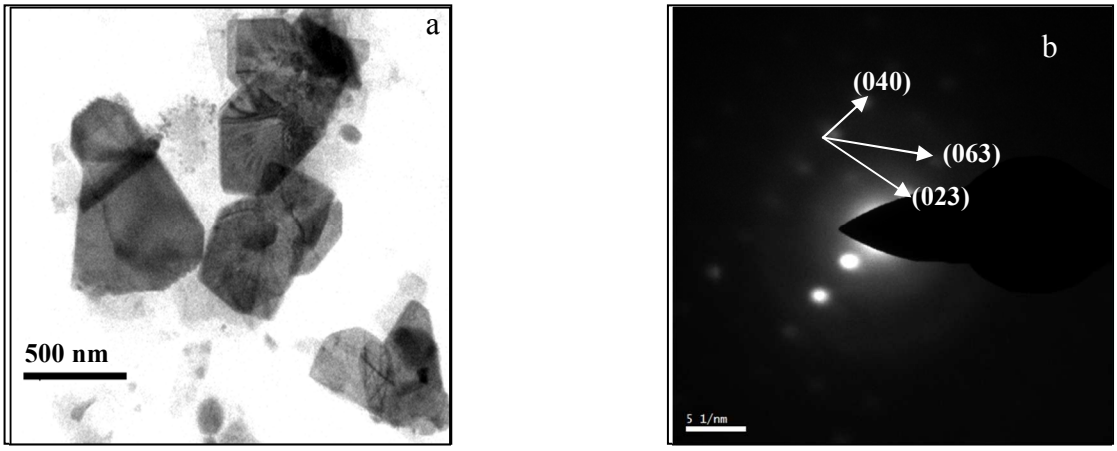


**Fig. 6** a) TEM image and b) SAED pattern of hexagonal SnS nanosheets prepared by thermolysis of $[Et_2Sn(2\text{-}SC_5H_4N)_2]$ (**2**) in OLA at 300 $^oC$ for 10 minutes.

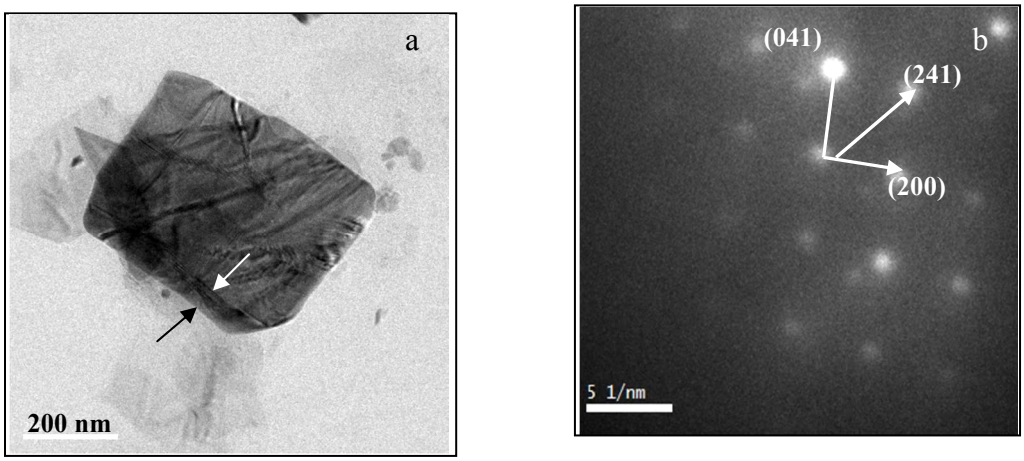


**Fig. 7** a) TEM image and b) SAED pattern of rectangular SnS nanosheets prepared by thermolysis of $[Et_2SnCl\{SC_4H(Me\text{-}4,6)_2N_2\}]$ (**5**) in OLA at 300 $^{o}$C for 5 minutes.

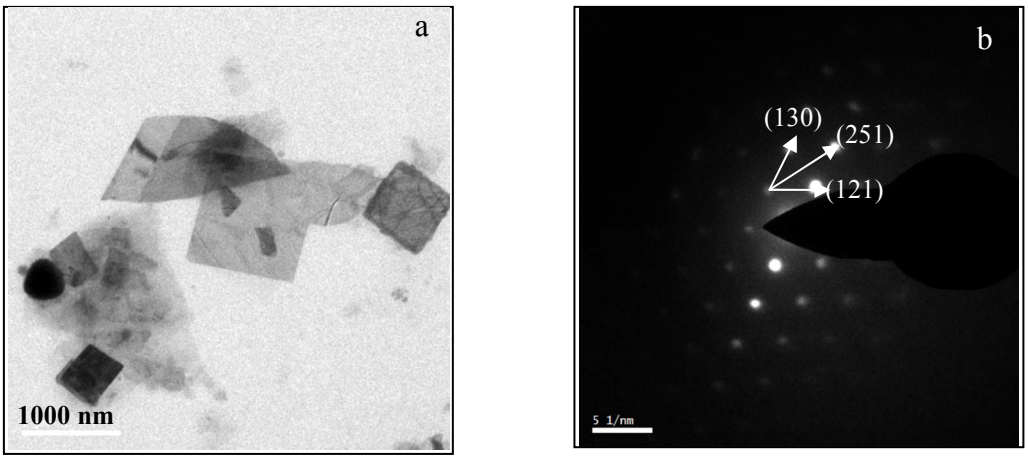


**Fig. 8** a) TEM image and b) SAED pattern of SnS nanosheets prepared by thermolysis of $[Et_2SnCl\{SC_4H(Me\text{-}4,6)_2N_2\}]$ (**5**) in TOPO-OLA at 320 $^oC$.

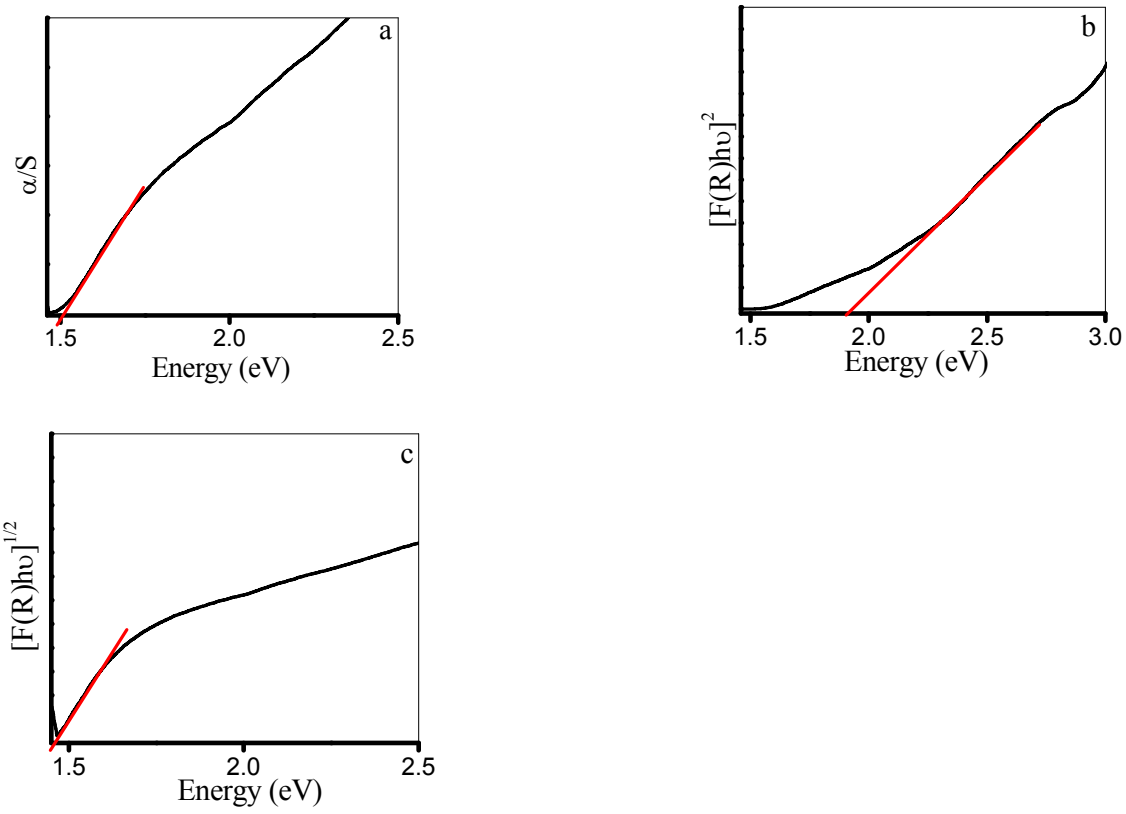


**Fig. 9** a) Solid-state diffuse reflectance spectrum of SnS rectangular sheets obtained by thermolysis of $[Et_2SnCl\{SC_4H(Me\text{-}4,6)_2N_2\}]$ (**5**) in OLA at 300 $^oC$ for 5 minutes and their Kubelka-Munk conversion plots of b) $[F(R)h\nu]^2$ vs energy and c) $[F(R)h\nu]^{1/2}$ vs energy from which direct and indirect band gaps were determined.

**Table of contents**

# Diorganotin(IV) 2-pyridyl and 2-pyrimidyl thiolates: Synthesis, structures and their utility as molecular precursors for the preparation of tin sulfide nanosheets

Adish Tyagi,[a] G. Kedarnath,*[a] Amey Wadawale,[a] Vimal K. Jain,*[a] Mukesh Kumar[b] and B. Vishwanadh[c]

Organotin complexes, $[R_2Sn(2\text{-}SC_5H_4N)_2]$ and $[R_2SnCl\{SC_4H(Me\text{-}4,6)_2N_2\}]$ (R = Me, Et) were prepared, characterized and utilized as ssps for the preparation of SnS nanosheets. The direct/indirect band gaps of the latter were evaluated.